

AMORPHOUS MATERIALS: PROPERTIES, STRUCTURE, AND DURABILITY

Nepheline structural and chemical dependence on melt composition

JOSÉ MARCIAL^{1,2}, JARROD CRUM³, OWEN NEILL⁴, AND JOHN MCCLOY^{1,2,*}

¹School of Mechanical and Materials Engineering, Washington State University, Pullman, Washington 99164, U.S.A.

²Materials Science and Engineering Program, Washington State University, Pullman, Washington 99164, U.S.A.

³Pacific Northwest National Laboratory, Richland, Washington 99352, U.S.A.

⁴Peter Hooper GeoAnalytical Laboratory, School of the Environment, Washington State University, Pullman, Washington 99164, U.S.A.

ABSTRACT

Nepheline crystallizes upon slow-cooling in some melts concentrated in Na₂O and Al₂O₃, which can result in a residual glass phase of low chemical durability. Nepheline can incorporate many components often found in high-level waste radioactive borosilicate glass, including glass network ions (e.g., Si, Al, Fe), alkali metals (e.g., Cs, K, Na, and possibly Li), alkaline-earth metals (e.g., Ba, Sr, Ca, Mg), and transition metals (e.g., Mn, and possibly Cr, Zn, Ni). When crystallized from melts of different compositions, nepheline composition varies as a function of starting melt composition. Five simulated high-level nuclear waste borosilicate glasses shown to crystallize large fractions of nepheline on slow-cooling were selected for study. These starting melt compositions contained a range of Al₂O₃, B₂O₃, CaO, Na₂O, K₂O, Fe₂O₃, and SiO₂ concentrations. Compositional analyses of nepheline crystals in glass by electron probe micro-analysis (EPMA) indicate that nepheline is generally rich in silica, whereas boron is unlikely to be present in any significant concentration, if at all, in nepheline. Also, several models are presented for calculating the fraction of vacancies in the nepheline structure.

Keywords: Nepheline, glass, vacancy, nuclear waste, crystallization, electron microprobe, nepheline crystal chemistry and structure

Lithium-containing nephelines have been synthesized with Li concentrations up to $\text{Na}_{0.85}\text{Li}_{0.15}\text{AlSiO}_4$ without converting to the different crystal structure of β -eucryptite (LiAlSiO_4) (Ota et al. 1995). Glasses containing a large fraction of B in $\text{NaB}_x\text{Al}_{(1-x)}\text{O}_4$ have been produced, but these were not crystallized to assess the possibility of fourfold-coordinated B entering the nepheline structure in place of Al (Pierce et al. 2010).

As a starting point for this work, the Inorganic Crystal Structure Database (ICSD, ver. 2013, <http://www.nist.gov/srd/nist84.cfm>), was searched, providing 26 nepheline data points with compositions and associated structural data. An additional 10 measured compositions were gathered from the literature (Krause et al. 2013; Matsumoto et al. 2014; Upadhyay 2012). Note that this sampling is by no means comprehensive; compositions that are more properly kalsilite or kaliophilite were not included. All of these data were normalized to 32 atoms of oxygen to plot the range of the major components shown in Figure 1; trace elements (<0.01 atoms per formula unit) were not plotted. The ideal stoichiometry for nepheline is $X_8Y_8\text{Si}_8\text{O}_{32}$, where $X = \text{Na}, \text{K},$ and Ca , $Y = \text{Al}$ and Fe . From this plot it is clear that when nepheline deviates from ideal it becomes silica rich, at the expense of the X and/or Y sites, as has been noted previously (Dollase and Thomas 1978; Donnay et al. 1959; Rossi et al. 1989). Both Na and K can be observed together in nepheline, but there are end-members that contain either Na (Na-nepheline) or K (kalsilite) (Deer et al. 2004). To a lesser extent, some Ca and Fe are observed in nepheline both in natural materials and in HLW waste glasses.

IMPORTANCE OF NEPHELINE FOR NUCLEAR WASTE PROCESSING

The Hanford Site in southeastern Washington State, U.S.A., contains a large volume of legacy high-level radioactive waste that will be immobilized in borosilicate glass at the Waste Treatment and Immobilization Plant (WTP) for ultimate disposal in a geologic repository. The major components of the waste vary

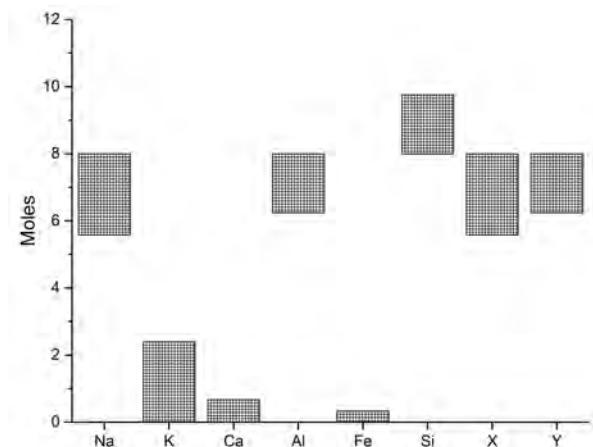


FIGURE 1. Nepheline major component composition ranges, normalized to 32 oxygen atoms, as taken from the ICDD and selected literature. In this figure, $X = \text{Na} + \text{K} + \text{Ca}$ and $Y = \text{Al} + \text{Fe}$. The values for X and Y were calculated from the compositional values reported for individual samples.

greatly due to the multitude of processes used over decades to produce and extract plutonium, creating a very large range of glass compositions, whose properties must be studied, modeled, and predicted accurately as a function of composition. Additionally, predictive glass property models derived from glass composition are necessary to ensure efficient processing, as well as acceptable waste form performance in the geologic repository. Within this vast compositional space, there are several clusters of wastes with similar compositions, and the largest of these is a high- Al_2O_3 waste that comprises approximately 47 vol% of the ~ 55 million gallons of Hanford waste (Kim et al. 2011). These high- Al_2O_3 clusters (~ 47 – 57 mass%) also contain simultaneously high concentrations of Na_2O (~ 12 – 16 mass%). This waste was generated when nuclear fuel cladding (Al) was dissolved in nitric and other acids, then basified with NaOH to reduce corrosion of waste storage tanks.

To maximize waste throughput at WTP and minimize cost of the clean-up mission, loading of waste in glass should be maximized along with melt rate, or conversion of waste plus glass forming feed chemicals (Fox et al. 2008; Hrma 2010). Maximizing waste loading in high- Al_2O_3 wastes often results in crystallization of nepheline (nominal composition NaAlSiO_4) upon slow cooling inside the storage canister. Crystallization of approximately ≥ 10 mass% of nepheline removes enough glass network formers and intermediates (i.e., Al_2O_3 , SiO_2 , and Fe_2O_3) to result in a residual glass phase that often has poor chemical durability due to enrichment in other network modifiers, transition metals, and boron (Bailey and Hrma 1995; McCloy and Vienna 2010a; Riley et al. 2001a, 2001b). Additionally, crystallization does not stop below the glass transition temperature (T_g) of the starting melt, as nepheline crystallization typically reduces the T_g of the remaining glass (Hrma 2010), especially for glasses containing a significant amount of boron oxide or when nepheline crystallizes with excess silica (Menkhaus et al. 2000). For this reason, it is important to accurately predict both the composition and amount of nepheline that crystallizes during cooling as a function of the starting melt composition so that (1) its impact on the final glass composition can be calculated, and (2) excessive nepheline formation can be avoided by modifying the starting melt composition.

Past studies have been conducted in compositional space where nepheline formation is anticipated (e.g., high Na_2O with high Al_2O_3 concentrations), in an effort to predict nepheline formation as a function of glass composition (Fox et al. 2008; Li et al. 2003, 1997; McCloy et al. 2015, 2011). The first conclusion of these studies was the establishment of an equation that can predict the absence of formation of nepheline based on the composition of the glass. The basic form of this predictive tool is called the nepheline discriminator (ND), and takes the form of $\text{SiO}_2/(\text{Na}_2\text{O} + \text{Al}_2\text{O}_3 + \text{SiO}_2) > 0.62$, where the glass composition in mass fraction is projected onto a normalized Al_2O_3 - Na_2O - SiO_2 ternary (Li et al. 2003, 1997). Glasses where $\text{ND} > 0.62$ are not expected to precipitate nepheline, as these compositions lie in the SiO_2 phase (tridymite/cristobalite/quartz), albite, sodium silicate ($\text{Na}_6\text{Si}_8\text{O}_{19}$, $\text{Na}_2\text{Si}_2\text{O}_5$), or mullite liquidus primary phase fields (Lambotte and Chartrand 2013). However, it has been observed that many glasses with $\text{ND} < 0.62$ also do not form nepheline, and thus this constraint conservatively limits glass composi-

tions to high normalized silica regions, effectively eliminating the advantage of high waste loading desirable for high- Al_2O_3 glasses (McCloy et al. 2011). From a geological standpoint, this is similar to the “quartz-normative” and “nepheline-normative” distinctions made in traditional studies of crystallization and liquid lines of descent in natural magmatic systems.

Of these glasses that fail the ND constraint, some do form a small fraction of nepheline, which does not negatively impact chemical durability (McCloy and Vienna 2010b) as measured by standard dissolution tests (ASTM 2008) on powdered samples. For this reason, additional studies were undertaken to further refine the relationship between composition and nepheline crystallization. The simplified ternary ND does not account for the composition effects of many other influential components, such as B_2O_3 , alkaline earths, and transition metals. A metric using calculated optical basicity (OB) (Duffy and Ingram 1976) to describe the average electronic environment of oxygen and hence its local bonding was developed to allow for contributions of all components, not just those on the reduced ternary (McCloy et al. 2011). The OB metric was used to complement the ND, and the combination of OB and ND was shown to be somewhat less conservative than ND alone, predicting additional compositions that would be free of nepheline formation (McCloy et al. 2011; Vienna et al. 2013).

Most recently, a neural network (NN) model was developed, based on a large database of existing data, that predicts the probability of nepheline formation based upon the component concentrations of Al_2O_3 , B_2O_3 , CaO , Li_2O , Na_2O , and SiO_2 (Vienna et al. 2013). Development of the NN model continues with the goal of ultimately predicting, based on the full starting melt composition, the actual volume fraction of nepheline formed upon canister centerline cooling (CCC), the slow-cooling profile estimated for the center of the glass in the HLW canister due to thermal mass and anticipated radioactive decay heating (Amoroso 2011; Rodriguez et al. 2011).

As these nepheline formation models are refined, they will become less conservative, allowing for increased waste loading. However, these models currently limit waste loading based upon a “go/no-go” designation; in other words, for a given glass composition, either nepheline is predicted to crystallize upon CCC (and hence the composition is unallowable) or it is not predicted to crystallize (and is allowable). However, the waste form durability is ultimately controlled by the impacts of nepheline crystallization on the residual glass composition, since it is assumed that the glass dissolution is faster than that of the mineral. This assumption has been shown by some to hold true for glasses vs. crystals of the same stoichiometry, e.g., albite ($\text{NaAlSi}_3\text{O}_8$)

(Bourcier 1998; Jantzen et al. 2010) but not by others (Hamilton et al. 2000). However, it is known that the topological structure of albite glass is typically different than that of albite mineral (McKeown 2005; Sugiyama et al. 1998; Taylor and Brown 1979; Taylor et al. 1980). Thus, next-generation models must be capable of predicting the fraction and composition of nepheline crystallized upon cooling and, thus, the residual glass composition as a function of starting melt composition. Additionally, in rare cases, it is possible that the residual glass structure could be more durable than the nepheline phase, and thus some prediction of the structure of the residual glass is desirable as well.

Riley et al. (2001a) calculated the residual glass composition based on the removal of components caused by crystallization of over 25 mineral types. The results showed reasonable agreement between the predicted response of the calculated residual glass composition and the measured response by the standard dissolution test. However, the crystallinity data used for this study was semi-quantitative, and the crystal compositions had to be generalized. These two factors lead to less accurate calculations of the residual glass composition, but the general idea was sound and only requires more precise crystal phase data to improve the calculation of the residual glass composition.

MATERIALS AND METHODS

Sample selection

A small set of HLW glasses subjected to the CCC profile heat treatment (Table 1) were selected for analysis by electron probe micro-analysis (EPMA). These samples were selected to compare nepheline composition to pre-crystallization melt composition and to determine whether Li and B were present in nepheline. These HLW glasses are typically initially melted at 1150 °C and quenched; the CCC heat treatment then brings the samples back to this melt temperature and provides a slow cooling, in this way simulating crystal growth from an initial melt.

Glass compositions were selected such that key nepheline components varied in concentration in an effort to see how glass composition impacts nepheline composition. All of the glasses measured except A4 had the same base composition and position on the normalized Al_2O_3 - Na_2O - SiO_2 ternary, but had increased concentrations of Li, Fe, K, or Ca while all other component ratios were held constant. Relative to the other glasses, A4 was much higher in Al, somewhat higher in B, depleted in Si, very depleted in Na, and high in Ca.

Microscopy and chemical analysis

Nepheline crystals grown in the experiments described above and mineral nepheline (Bancroft, Ontario, obtained from Ward’s Scientific, no. 46E5580) were imaged using scanning electron microscopy (SEM) with a backscattered electron (BSE) detector. These were further analyzed by EPMA for the concentrations of Al, B, Ca, Fe, K, Mg, Na, and Zr in nepheline crystals, using wavelength-dispersive X-ray spectroscopy (WDS). Measurements were performed on the largest observed nepheline branches. Since nepheline should not contain measurable Zr, ZrO_2 was analyzed to discriminate between the crystal and glass, thus accounting for the activation volume of the electron beam where it might have inadvertently encountered the Zr-bearing glass in addition to the

TABLE 1. Theoretical (as-batched starting) glass composition (mass%); and nepheline crystallinity (vol%) upon CCC heat treatment (from Rietveld analysis of X-ray diffraction patterns as obtained from the reference)

Glass ID	Ref	Nepheline	Al_2O_3	B_2O_3	CaO	Fe_2O_3	K_2O	Li_2O	MgO	Na_2O	P_2O_5	SiO_2	ZrO_2	Others*
A4	(Hrma et al. 2010)	21	24.02	11.99	6.08	5.91	0.14	6.77	0.12	9.59	1.05	30.51	0.40	3.42
NP-K-2	(Li et al. 1997)	48	12.95	7.53	1.05	9.35	6.00	4.23	0.64	19.08	0.94	36.12	0.27	1.84
NP-Ca-2	(Li et al. 1997)	26	12.52	7.28	10.00	9.05	0.09	4.10	0.62	18.46	0.91	34.94	0.26	1.77
NP-Fe-3	(Li et al. 1997)	32	13.31	7.74	1.08	12.95	0.10	4.35	0.66	19.62	0.94	37.14	0.28	1.83
NP-Li-2	(Li et al. 1997)	35	13.26	7.71	1.08	9.58	0.10	8.00	0.66	19.53	0.96	36.98	0.28	1.86
Minimum			12.52	7.28	1.05	5.91	0.09	4.1	0.12	9.59	0.91	30.51	0.26	1.77
Maximum			24.02	11.99	10.00	12.95	6.00	8.00	0.66	19.62	1.05	37.14	0.40	3.42

*The reader is referred to the original reference for the full composition, but the “others” category consists of varying amounts of Ag_2O , As_2O_3 , BaO , Bi_2O_3 , CdO , Cr_2O_3 , CuO , F , MnO , NiO , PbO , Sb_2O_3 , SeO_2 , SO_3 , SrO , TiO_2 , and ZnO .

crystal. Analyses that intersected the glass were considered spurious, and are not reported or considered here. In addition, semiquantitative energy-dispersive spectroscopy (EDS) was also performed to analyze the composition of regions whose composition deviated from the seven components analyzed through WDS.

For EPMA-WDS analyses, samples were thin-sectioned and polished to a 1 μm diamond finish. Samples were analyzed on a JEOL JXA-8500F field-emission electron microprobe equipped with Probe for EPMA analytical software (Donovan 2014). Analyzed elements, counting times, and standards are listed in Table 2; beam conditions were as follows: 15 keV accelerating voltage, 8 nA probe current, and 7 μm spot size. Linear off-peak backgrounds were used for all elements except Na (exponential fit) and B (polynomial fit). Oxygen was calculated stoichiometrically assuming common oxides Al_2O_3 , B_2O_3 , CaO , Fe_2O_3 , K_2O , MgO , Na_2O , SiO_2 , P_2O_5 , and ZrO_2 , then normalizing the measured nepheline composition, by mole, to 32 oxygen atoms.

Analysis of B was performed using a Cr/C synthetic multilayer layered dispersion element (LDE) analyzing crystal (LDE6, $2d = 120 \text{ \AA}$). While the LDE6 has a lower sensitivity for B, it was preferred to the Mo/B₄C LDE (LDEB, $2d = 148 \text{ \AA}$) (McGee et al. 1991; Raudsepp 1995) due to the B signal produced by fluorescence of the B in the analyzing crystal, which can nonsystematically contribute an excess of up to $\sim 0.5 \text{ wt\% B}_2\text{O}_3$ (Kobayashi et al. 1995; McGee and Anovitz 1996) and render any attempts to quantify low concentrations of B impossible. Additionally, the $\text{BK}\alpha$ peak, when measured using LDEB and LDE6 diffracting crystals, is located in a region of the continuum with upward concavity. As a result, careful spectrometer scans over both the peak and background positions had to be performed to accurately model the continuum shape, and to check for any spectral overlaps (such as those mentioned above) between higher order lines and both the peak and background positions. Silicon and aluminum are strong boron X-ray absorbers, and therefore the B X-ray yield is comparatively very small, while the matrix absorption correction for B analyses in aluminosilicate materials can be very large (McGee and Anovitz 1996).

Measurements of B were made in differential pulse-height analyzer mode to eliminate potential interferences from the third-order $\text{OK}\alpha$, second-order $\text{CaL}\alpha$, and fourth-order $\text{FeL}\alpha$ X-ray lines. Repeated measurements suggest that the B content of the analyzed nephelines do not exceed lower limit of detection (0.6 wt% B_2O_3 , calculated after Donovan 2014).

X-ray maps, showing relative compositional variations over certain sample areas, as well as compositions of additional phases, were obtained via energy-dispersive X-ray spectroscopy (EDS) using the WSU JEOL JXA-8500F electron microprobe. X-ray intensities were measured using a ThermoScientific UltraDry EDS detector, and compositions obtained from raw intensities using the PROZA $\phi(\rho z)$ matrix correction algorithms, similar to those of Bastin and Heijligers (1991), incorporated in the ThermoNORAN System7 analytical software. Due to the serious issues with EDS data quality (Horny et al. 2010; Newbury 2005; Newbury and Ritchie 2013; Newbury et al. 1995), especially “standardless” EDS quantification, this data should be regarded semi-quantitative at best, but it is sufficient to identify the major elemental components of these additional phases.

RESULTS

Microstructure and chemical imaging

Microstructures of the five samples obtained through SEM-BSE imaging are shown in Figure 2. BSE imaging demonstrates the presence of spinel and other as-yet unidentified phases all connected by a residual glass matrix. Table 3 provides the compositions of the spinel and the unidentified phase present in A4 after CCC heat treatment as measured through semi-quantitative EDS. The spinel phase in A4-CCC was high in iron and chromium, while the unidentified phase was high in aluminum and silicon and contained some phosphorus. Further understanding of the effect of glass composition on the composition of spinel is beyond the scope of this study, and the reader is referred to other works on this subject (Hrma et al. 2014; Jantzen and Brown 2007a; Matyáš et al. 2010). Note that nepheline grows in dendritic patterns with relatively close spacing of less than the width of an individual branch between neighboring dendrites, suggesting substantial undercooling, which is both thermal and

TABLE 2. Spectrometer conditions and standard assignments for WDS measurements of A4, NP-K-2, and NP-Fe-3

Element/ X-ray line	Analyzing crystal	On-peak count time (s)	Low-peak count time (s)	High-peak count time (s)	WDS standards
$\text{AlK}\alpha$	TAP	20	10	10	Anorthite, USNM 13741 (A4, neph mineral) Hornblende, Wilburforce (NP glass)
$\text{BK}\alpha$	LDE6	240	120	120	K-490 NIST Glass
$\text{CaK}\alpha$	PETJ	20	10	10	Diopside 1, C.M. Taylor Corp.
$\text{FeK}\alpha$	LiF	240	120	120	Hornblende, Wilburforce
$\text{KK}\alpha$	PETH	60	30	30	Hornblende, Kakanui, USNM 143965
$\text{MgK}\alpha$	TAP	150	75	75	Diopside 1, C.M. Taylor Corp.
$\text{NaK}\alpha$	TAP	20	10	10	Albite 4, C.M. Taylor Corp.
$\text{SiK}\alpha$	TAP	20	10	10	K-412 NIST Glass
$\text{ZrL}\alpha$	PETH	120	60	60	Zircon no. 1, C.M. Taylor Corp.

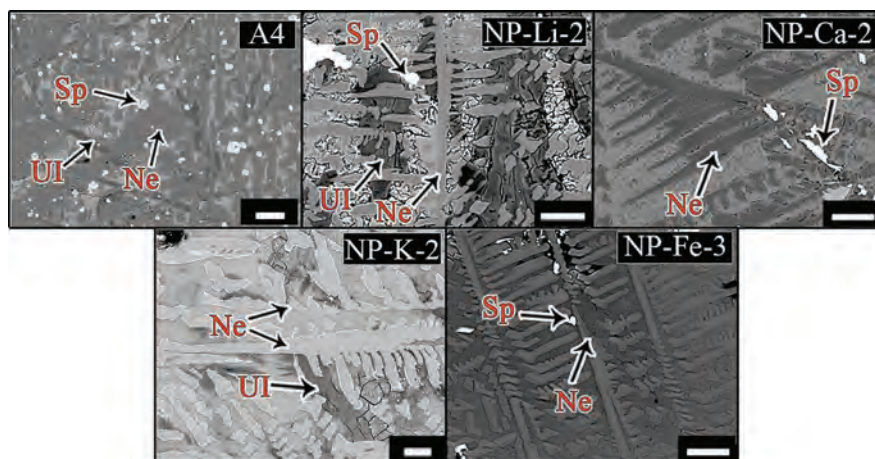


FIGURE 2. SEM BSE micrographs of the five HLW glasses after CCC heat treatment; the scale bar is 25 μm . The overlaid text denotes the position of the phases nepheline (Ne), spinel (Sp), and unidentified (UI). (Color online.)

compositional, since the composition of nepheline is different than the starting melt (Kirkpatrick 1975).

In the BSE images, the spinel phase appears completely white. As is well known, in backscatter electron images, grayscale value is proportional to the mean atomic number (A) – bright = high mean A , dark = low mean A . To use BSE to see the variations in composition of phases with very similar mean A , it is necessary to acquire the images at high grayscale contrast, which means phases with much higher mean A (i.e., spinel compared to nepheline and borosilicate glass) will look entirely white, as all pixels will have grayscale values higher than the maximum contrast threshold. Additionally, when comparing the BSE images in Figure 2 there is an apparent variance in brightness of the nepheline branches of each sample. Additional factors known to affect the brightness are the beam parameters that are set during image acquisition to provide good image quality.

Nepheline chemical compositions

The mean nepheline compositions were converted to elemental mole fraction, with total oxygen calculated stoichiometrically based on assumed valence states of analyzed cations (Al^{3+} , B^{3+} , Fe^{3+} , Na^{1+} , K^{1+} , Ca^{2+} , and Si^{4+}). From this data, the chemical formula for each nepheline was determined by grouping elements into sites based on Goldschmidt's rules of substitution (Goldschmidt 1937) (Table 4; Fig. 3). The ideal nepheline formula is

TABLE 3. Measured compositions of unidentified (UI) phase and spinel in A4 CCC by semi-quantitative energy-dispersive spectroscopy

Analyte	UI ^a	Spinel ^a
Na ₂ O	0.52 ± 0.08	
MgO	0.72 ± 0.10	0.62 ± 0.12
Al ₂ O ₃	26.45 ± 0.26	7.22 ± 0.17
SiO ₂	55.83 ± 0.53	1.32 ± 0.13
P ₂ O ₅	12.61 ± 0.27	
Fe ₂ O ₃	3.88 ± 0.39	61.95 ± 1.40
Cr ₂ O ₃		18.48 ± 0.41
NiO		10.41 ± 0.70
Total	100.00	100.00

^a wt%.

TABLE 4. Nepheline compositions measured by EPMA-WDS (top: wt% oxides; bottom: molar cation proportions, normalized to 32 oxygen atoms per formula unit)

		wt% Oxides					Total			Molar Cation Proportions (normalized to 32 oxygen atoms)				Total
		SiO ₂	Al ₂ O ₃	Fe ₂ O ₃	MgO	CaO	Na ₂ O	K ₂ O		Site X	Site Y	Site Z		
		X Total	Na	K	Ca	Mg	Y Total	Al	Fe	B	Si	O		
A4	Average	7.30	6.94	0.06	0.31	0.00	7.98	7.79	0.19	0.00	8.12	32	55.39	
	St.Dev.		0.35	0.00	0.02	0.00		0.09	0.08		0.10			
NP-K-2	Average	8.19	5.94	2.23	0.00	0.03	7.95	6.82	1.13	0.00	7.98	32	56.13	
	St.Dev.		0.05	0.02	0.00	0.01		0.23	0.19		0.04			
NP-Fe-3	Average	7.96	7.87	0.05	0.01	0.02	7.75	6.20	1.55	0.00	8.19	32	55.90	
	St.Dev.		0.04	0.00	0.00	0.00		0.04	0.03		0.02			
NP-Ca-2	Average	8.34	8.12	0.01	0.13	0.07	7.68	6.89	0.79	0.00	8.12	32	56.14	
	St.Dev.		0.15	0.00	0.08	0.01		0.10	0.04		0.06			
NP-Li-2	Average	8.12	8.03	0.07	0.01	0.01	7.78	6.82	0.96	0.00	8.13	32	56.03	
	St.Dev.		0.20	0.00	0.01	0.01		0.11	0.06		0.07			

$X_aY_bZ_c\text{O}_{32}$; where $X = \text{Na, K, Ca, and/or Mg}$; $Y = \text{Al, Fe, and/or B}$; and $Z = \text{Si}$. Note that this formula is used to account for composition only as determined by EPMA-WDS, not crystallographic site occupancy. Vacancies, when they occur, are in the ring channels (X sites) and not in the tetrahedral sites (Y and Z sites), as elaborated in the Discussion.

EPMA analysis (Table 3) showed that nepheline crystals in A4 and NP-Fe-3 were enriched in Si (Site $Z > 8$) and alkali-deficient (Site $X < 8$) compared to ideal nepheline stoichiometry (Site $Z = \text{Site } X = 8$). Nepheline crystals in NP-K-2, on the other hand were found to be relatively Si-deficient (Site $Z < 8$) and alkali-rich (Site $X > 8$). Fe and potentially B are believed to substitute for Al on the Y -site as a function of their concentration in the melt (McCloy et al. 2015). For example, as Al_2O_3 is replaced by Fe_2O_3 or B_2O_3 in the glass, then the concentration Fe or B increases at the expense of Al in the nepheline phase.

The average composition of the nepheline measured by EPMA was significantly different than the ideal natural nepheline $\text{K}_{0.25}\text{Na}_{0.75}\text{AlSiO}_4$, particularly due to the low K levels in these glasses. Figure 3 shows a comparison of the determined composi-

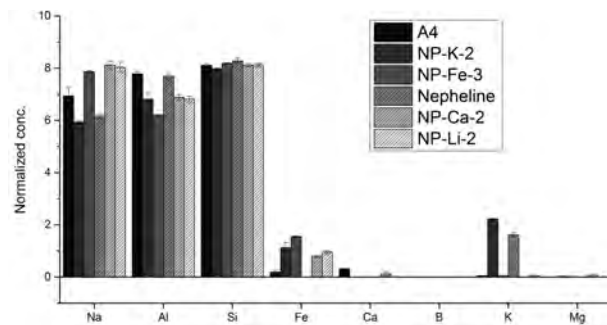


FIGURE 3. Measured nepheline compositions for A4, four NP glasses, and a nepheline standard, with element concentrations normalized to 32 oxygen atoms and ignoring any vacancies. “Nepheline” indicates the natural Bancroft, Ontario, sample.

tions of the nepheline crystals. Only the NP-K-2 glass produced nepheline close to the ideal natural nepheline stoichiometry.

Residual glass compositions

Figure 4 displays the difference between the nepheline composition measured through EPMA-WDS and the nominal glass. Of course, the residual glass computed here assumes no other crystalline phases are present, which is clearly not the case. However, we still believe this calculation is valuable, as nepheline is the dominant crystalline phase in the glasses, and the residual glass is computed based on actual measured nepheline composition, rather than assuming a nominal “nepheline” as NaAlSiO_4 , as is usually done (McCloy et al. 2015; Riley et al. 2001b). As an example, the nepheline that formed from NP-K-2 after CCC heat treatment can be written as $(\text{Na}_{0.74}\text{K}_{0.28})(\text{Al}_{0.85}\text{Fe}_{0.14})\text{Si}_{1.00}\text{O}_4$ and shows lower enrichment of Na in the crystal relative to the other samples, due to the availability of K to enter the nepheline ring sites. By contrast, all other samples had low K in the starting melt and hence required more Na to go into the nepheline crystals. However, the situation is in reality more complex as shown in the X-ray map in Figure 5. The K map shows enrichment in the crystal as expected, but the Na map suggests higher Na in the residual glass immediately next to the crystal, which is not expected. Additionally, Na is notably absent in the Si-rich unidentified phase. In general, the area surrounding the nepheline crystals is depleted in both Al_2O_3 and SiO_2 relative to the nepheline (i.e., the grayscale is darker in the glass relative to the crystals, which are most easily seen in the Al and K maps). Furthermore, since nepheline does not appear to accept B_2O_3 based on our current results, the resulting residual glass phase is enriched in boron and transition metals relative to the starting melt composition, as the nepheline crystals push out these elements.

DISCUSSION

Vacancy estimation

When mineral compositional data are presented from EPMA-WDS data, it is typically normalized using to an ideal chemical formula; vacancy concentration is usually ignored. Assessments of

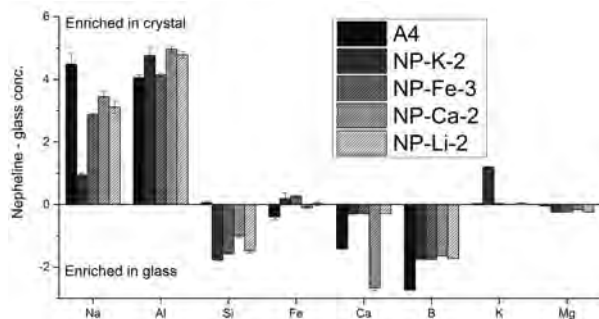


FIGURE 4. Predicted difference between nepheline compositions and starting melt compositions, with concentration normalized to 32 oxygen. Enrichment in the nepheline relative to starting melt shows as positive, and depletion in nepheline relative to the starting melt shows as negative. Error bars represent the standard deviation determined by measurement through EPMA.

vacancy concentration can only be made, then, by using a charge-balancing structural model or by performing careful synchrotron or neutron diffraction experiments on suitable samples. As the latter option is not viable for our crystallized glasses containing multiple species, a structural model must be used. We go over these calculations in some detail as follows as the assumptions and calculations are rarely discussed carefully in the literature.

As described previously, cationic vacancies in the nepheline structure ensure charge balance when nepheline contains Ca or is Si-rich. In the former case, if sufficient Ca partitions into nepheline, a large number of vacancies are created and the amount of Na removed from the glass by crystallization is reduced. By this mechanism, Na may be enriched in the residual glass. In the latter case, more Si than Al is in nepheline, requiring vacancies for charge compensation, and relatively more depletion of Si in the residual glass. This simplification does not take into account the effects of secondary phases, which are found in the microstructures of HLW glasses after CCC heat treatment. The effects of extraction of alumina and silica by nepheline with the enrichment of alkali and boron in the residual glass contribute to the reduction of residual glass durability.

Three methods were followed to estimate the concentration of vacancies in the analyzed samples. In all cases, calculations were performed with all formula units normalized to 32 oxygen atoms. Two methods are from Rossi et al. (1989). In this work, Rossi et al. consider a compositional space for many stuffed derivatives of cristobalite and tridymite. This compositional space may be illustrated as a tetrahedron (Fig. 6) with vertices representing the compounds of anorthite ($\square_4\text{Ca}_4\text{Al}_8\text{Si}_8\text{O}_{32}$), Na-nepheline/carnegieite ($\text{Na}_8\text{Al}_8\text{Si}_8\text{O}_{32}$), kaliophilite/kalsilite ($\text{K}_8\text{Al}_8\text{Si}_8\text{O}_{32}$), and tridymite/cristobalite ($\square_8\text{Si}_{16}\text{O}_{32}$) (Rossi et al. 1989). Three axes of the tetrahedron represent so-called cation exchange vectors designated as r , p , and q (Rossi et al. 1989). The corresponding exchanges (denoted as = below), modified for the potential presence of major HLW glass components B, Fe, and Mg, are as follows:

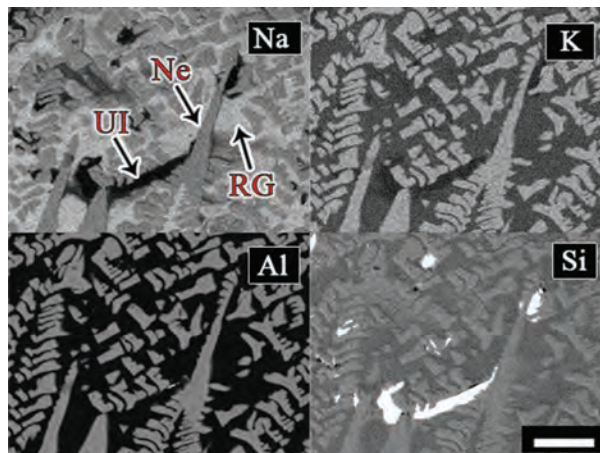


FIGURE 5. SEM-EDS map of the microstructure of NP-K-2 after CCC heat treatment showing the relative abundance of Si, Na, K, and Al in grayscale (dark = low abundance, bright = high abundance); the scale bar is 50 μm . UI = unidentified phase, Ne = nepheline, and RG = residual glass. (Color online.)

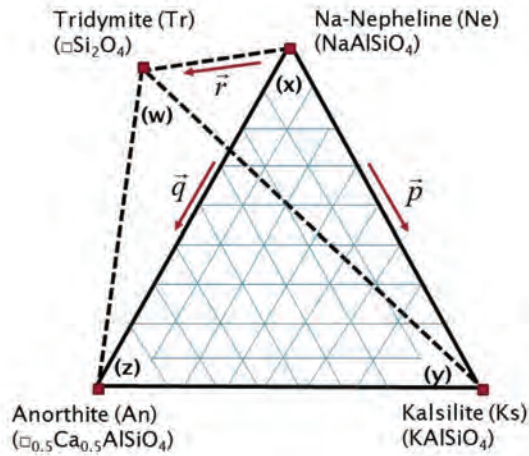


FIGURE 6. Illustrative comparison of the $\square_{0.5}\text{Ca}_{0.5}\text{AlSiO}_4$ - $\text{Na}_8\text{Al}_8\text{Si}_8\text{O}_{32}$ - $\text{K}_8\text{Al}_8\text{Si}_8\text{O}_{32}$ - $\square_{0.5}\text{Si}_2\text{O}_4$ tetrahedron following the work of Blancher et al. and Rossi et al. described in the text for the calculation of vacancy concentration. The parameters for the Rossi et al. (1989) method are shown as vectors r , q , and p and the parameters for the Blancher et al. (2010) method are shown in parentheses as constants w , x , y , and z . (Color online.)

$$(p): \text{Na} = \text{K}$$

$$(q): 2\text{Na} = (\text{Ca} + \text{Mg}) + \square$$

$$(r): \text{Si} + \square = (\text{Al} + \text{Fe} + \text{B}) + \text{Na}.$$

These exchanges proceed to charge-compensate the nepheline structure upon substitution. Following these assumptions, a composition for nepheline as proposed by Rossi et al. (1989) for natural nephelines and modified for potential B, Fe, and Mg may be considered as



The first calculation method provided in this work, designated *Rossi-1*, assumes (1) that the r coefficient can be calculated from the measured Na concentration rather than from the measured Si concentration (the latter is assumed in *Rossi-2*) and (2) that of the three species (Al, Fe, and B) that could be assigned to the available Y-sites, all Al must be used. Any unassigned Y-sites would then be divided equally among the measured Fe and B. The latter assumption was to ensure that all Al was four-coordinated Al in nepheline and that Al constituted the majority of the Y-site species. The *Rossi-1* calculation proceeded as follows:

- (1) Normalize analyte concentrations to accommodate 32 oxygen atoms.
- (2) Normalize all potential tetrahedrally coordinated cations (Si, Al, Fe, and B) to 16.
- (3) Solve for r , p , and q :
 - $r = 8 - 2(\text{Ca} + \text{Mg}) - \text{K} - \text{Na}$
 - $p = \text{K}$
 - $q = \text{Ca} + \text{Mg}$.
- (4) Multiply B and Fe by $(8 - r)/(\text{Al} + \text{Fe} + \text{B})$ based on the assumptions above.

- (5) Assume the concentration of Mg and Ca is that measured through EPMA.
- (6) Solve for the remaining components based on Equation 1.

Table 5 provides the composition of nepheline determined through the *Rossi-1* method. The first point of discussion arising from this method involves assumption (1); following step 3 above, where r is determined from the Na concentration, generates a negative vacancy concentration in samples NP-K-2, NP-Ca-2, and NP-Li-2. As a result of this, it is believed that computing r from measured alkali concentrations can result in unphysical values for some compositions. In the next method, *Rossi-2*, r is deduced from the measured silica concentration, and here becomes a positive value for all samples. As will be discussed later, assumption (2) artificially increased the concentration of Al in the *Rossi-1* method.

As previously mentioned, the *Rossi-2* method was also differentiated, which assumes (3) the r coefficient can only be obtained from the measured Si concentration, (4) the ratio of Al, B, and Fe that may be assigned to the available Y-sites is the same as the ratio initially measured through WDS, and (5) that Ca and Mg both enter the same site, so the fractions of Ca and Mg must be back-calculated from the q coefficient. Table 6 provides the composition of nepheline determined through the *Rossi-2* method. The *Rossi-2* calculation is performed as follows:

TABLE 5. Nepheline composition following the *Rossi-1* method described in the text

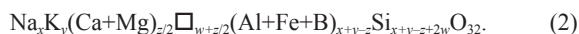
	A4	NP-K-2	NP-Fe-3	Nepheline	NP-Ca-2	NP-Li-2
Na	6.90	5.96	7.49	6.18	8.22	8.08
Al	7.57	8.26	7.61	7.82	8.65	8.19
Si	8.43	7.74	8.39	8.18	7.35	7.81
Fe	0.18	1.18	1.52	0.01	0.89	1.01
Ca	0.31	0.03	0.03	0.01	0.21	0.02
B	0.00	0.00	0.00	0.00	0.00	0.00
K	0.05	2.24	0.05	1.62	0.01	0.07
Mg	0.00	0.03	0.02	0.00	0.07	0.01
Total	23.44	25.43	25.13	23.82	25.41	25.19
O	32	32	32	32	32	32
Vacancy	0.74	-0.23	0.42	0.19	-0.44	-0.17
r	0.43	-0.26	0.39	0.18	-0.65	-0.19
p	0.05	2.24	0.05	1.62	0.01	0.07
q	0.31	0.03	0.03	0.01	0.21	0.02

TABLE 6. Nepheline composition following the *Rossi-2* method described in the text

	A4	NP-K-2	NP-Fe-3	Nepheline	NP-Ca-2	NP-Li-2
Na	7.26	5.69	7.66	6.07	7.35	7.71
Al	7.74	6.85	6.22	7.70	6.98	6.85
Si	8.07	8.02	8.22	8.29	8.22	8.18
Fe	0.19	1.14	1.56	0.01	0.80	0.97
Ca	0.31	0.00	0.00	0.01	0.08	0.01
B	0.00	0.00	0.00	0.00	0.00	0.00
K	0.05	2.24	0.05	1.62	0.01	0.07
Mg	0.00	0.02	0.02	0.00	0.03	0.01
Total	23.62	23.95	23.73	23.70	23.48	23.79
O	32	32	32	32	32	32
Vacancy	0.38	0.05	0.25	0.30	0.43	0.20
r	0.07	0.02	0.22	0.29	0.22	0.18
p	0.05	2.24	0.05	1.62	0.01	0.07
q	0.31	0.03	0.03	0.01	0.21	0.02

- (1) Normalize analyte concentrations to accommodate 32 oxygen atoms.
- (2) Normalize all potential tetrahedrally coordinated cations (Si, Al, Fe, and B) to 16.
- (3) Solve for r , p , and q :
 - $r = \text{Si}-8$
 - $p = \text{K}$
 - $q = \text{Ca}+\text{Mg}$.
- (4) Multiply Al, B, and Fe by $(8-r) \cdot x_i / (\text{Al}+\text{Fe}+\text{B})$ based on the assumptions above where $x_i = \text{Al}$, B, or Fe, respectively.
- (5) Multiply Ca, Mg by y_i/q where $y_i = \text{Ca}$ or Mg, respectively.
- (6) Solve for the remaining components based on Equation 1.

As an alternative, a least-squares fit of the compositional data to the general formula for a solid solution of $An(\square_{0.5}\text{Ca}_{0.5}\text{AlSiO}_4)$, hexagonal nepheline (NaAlSiO_4) (*Ne*), *Ks* (KAlSiO_4), and *Qz* (Si_2O_4), can be performed as described by Blancher et al. (2010). The abbreviations of *An*, *Ks*, and *Qz* applied herein refer to the composition rather than to a particular mineralogical phase. The general formula based on the EPMA data was hypothesized as:



This method was employed to explicitly include the possibility of Ca and Mg occupying the X-site and Fe and B (in addition to Al) occupying the Y-site. In this modified formula it is assumed that Ca^{2+} and Mg^{2+} enter the Na^+ site resulting in a K^+ site vacancy, and that Al, Fe, and B occupy Al sites, denoted as T(1) or T(4) sites (Blancher et al. 2010). The merit function minimized for this calculation was D^2 , see below. The parameters x , y , z , and w represent the fractions of Ne, Ks, An, and Qz (Blancher et al. 2010). Boundary conditions for the fit were: $x \leq \text{Na}$, $y \leq \text{K}$, and $z/2 \leq (\text{Ca}+\text{Mg})$. Substituting the resulting fit parameters into Equation 2, the calculated nepheline compositions are shown in Table 7. The significance of this data is that a general formula for nepheline was derived to include the occupancy of boron in the T(1) and T(4) sites. The assumption that Fe enters the tetrahedral Al site follows the work of Donnay et al. (1959) and Tait et al. (2003).

The Blancher et al. (2010) least-squares method to solve

for vacancy concentration follows the works of Donnay et al. (1959) and Deer et al. (2004). When this method is modified for Mg, Fe, and B the steps for performing this calculation become:

- (1) Normalize analyte concentrations to accommodate 32 oxygen.
- (2) Least-squares fit x , y , z , and w by finding a minimum of the fit coefficient, D^2 (modified to include Fe, B, and Mg). Five constraints were implemented in the fitting of data.

$$D^2 = (\text{Na} - x)^2 + (\text{K} - y)^2 [\text{Al} + \text{Fe} + \text{B} - (x + y + z)]^2 +$$

$$\left(\text{Ca} + \text{Mg} - \frac{z}{2} \right)^2 + (\text{Si} - (x + y + z + 2w))^2$$

- (a) $x \leq \text{Na}$
- (b) $y \leq \text{K}$
- (c) $z/2 \leq (\text{Ca}+\text{Mg})$
- (d) The ratio of Ca and Mg was maintained constant. To achieve this, measured WDS values for Ca and Mg were multiplied by $z/2(\text{Ca}+\text{Mg})$.
- (e) The ratio of Al, B, and Fe was maintained constant. To achieve this, measured WDS values for Al, Fe, and B were multiplied by $(x+y+z)/(\text{Al}+\text{Fe}+\text{B})$.

In this modified method, the z parameter is halved because each mole of *An* produces half a mole of Ca or \square ; however, for the calculation of Al and Si, z is not halved since each mole of *An* produces one mole of Al or Si. Similarly, the w parameter must be multiplied by two for the calculation of Si but not for \square . Constraints (c) and (d) were used to maintain a constant ratio of Ca:Mg in the Na site and Al:Fe:B in T(1) or T(4) sites. Two points of discussion arise from this calculation: (1) constraint (d) changes the Si/Al ratio and (2) this calculation does not account for Na and Ca in the K site and \square in the Na site, as had been described by Rossi et al. (1989) and Tait et al. (2003).

The anorthite, Na-nepheline/carnegieite, kaliophilite/kalsilite, and tridymite/cristobalite quaternary as described by Rossi et al. (1989) is shown in Figure 6. This tetrahedron was modified to allow for comparison to the parameters of the Blancher method (Blancher et al. 2010). Results of comparison of these three methods are shown in Tables 5–7. Figure 7 provides the comparison of the calculated nepheline compositions for the five simulant nuclear waste glasses and the mineral sample as calculated through the preferred Rossi-2 method. Among the three methods, the Rossi-1 method overestimates the concentration of Al in the high-Fe NP glasses, but the calculated Fe concentration is approximately equivalent to the other two methods. It is believed that this is because step 4 of Rossi-1 artificially increases the amount of Al at the expense of available Fe and B. However, the calculated Na and K concentrations show no clear trend of enrichment as would be required for charge compensation. The Rossi-1 method also predicts a negative vacancy concentration for NP-K-2. Comparison of the Rossi-2 and Blancher methods reveals that the Blancher method predicts higher vacancy concentrations in A4 and NP-Fe-3 despite calculating approximately the same K concentration as the Rossi-2 method. The Blancher method was also found to estimate a greater fraction of Al and Fe than what was measured with EPMA-WDS. The Rossi-2 calculation also predicts slightly higher Na levels in NP-Fe-3, NP-Ca-2,

TABLE 7. Least-squares fit nepheline composition following the Blancher et al. method described in the text

	A4	NP-K-2	NP-Fe-3	Nepheline	NP-Ca-2	NP-Li-2
Na	6.94	5.76	7.81	6.13	7.80	7.85
Al	7.43	6.83	6.25	7.72	7.12	6.90
Si	8.12	7.98	8.19	8.28	7.93	8.13
Fe	0.18	1.14	1.56	0.01	0.82	0.98
Ca	0.31	0.00	0.00	0.01	0.04	0.01
B	0.00	0.00	0.00	0.00	0.00	0.00
K	0.06	2.21	0.00	1.58	0.00	0.00
Mg	0.00	0.00	0.00	0.00	0.02	0.01
Total	23.03	23.92	23.81	23.73	23.74	23.86
O	32	32	32	32	32	32
Vacancy	0.56	0.01	0.19	0.28	0.07	0.14
w	0.25	0.01	0.19	0.27	0.00	0.13
x	6.94	5.76	7.81	6.13	7.80	7.85
y	0.06	2.21	0.00	1.58	0.00	0.00
z	0.62	0.00	0.00	0.02	0.13	0.03
D^2	0.13	0.03	0.01	0.00	0.22	0.05

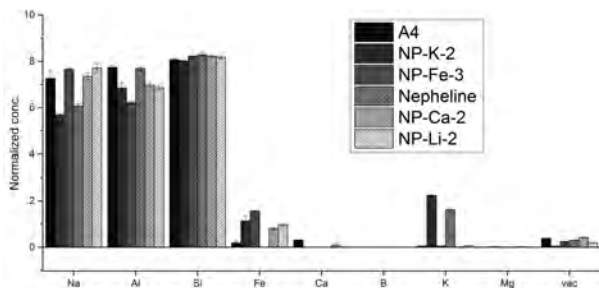


FIGURE 7. Comparison of the calculated nepheline concentration as determined through the *Rossi-2* calculation method described in the text. Data was normalized to 32 oxygen atoms. The error bars indicate the measured standard deviation. “Nepheline” indicates the natural Bancroft, Ontario, sample.

and NP-Li-2 when considering measurement error. This model could be predicting a reduction in vacancy concentration by the introduction of Na and Ca into the larger hexagonal nepheline channel normally filled by K or vacancies. In their work, Rossi et al. (1989) suggested that their calculation method assumed no site preference for Ca atoms and that the large hexagonal rings could be treated as two different sites where K, Na, Ca, and vacancies could be simultaneously found in varying abundance. The *Rossi-2* method has been used here to show the trends for calculated nepheline composition because it does not introduce additional error due to fitting, while still providing positive values for the r , p , and q coefficients.

Nepheline structural and compositional dependence on melt composition

A few observations can be made regarding the selectivity of nepheline crystals given different available starting melt compositions. It is significant that despite the higher concentration of Ca in NP-Ca-2, more Ca went into the nepheline precipitated from A4 (see Fig. 3). Recall that A4 was also very alkali-deficient ($X \sim 7$ when not counting Ca), so the availability of other cations for charge compensation forced the crystal to accept the less-preferred Ca, at the expense of a high cation vacancy concentration. Additionally, despite differences in starting alkali and alkaline earth concentrations, nepheline compositions for NP-Ca-2 and NP-Li-2 had very similar overall compositions, similar Fe levels, and very little Ca and K substitution. However, typical EPMA systems cannot detect lithium as is well known.

Measured nepheline compositions for both NP-K-2 and NP-Fe-3 were relatively enriched in Fe compared to their starting melt compositions (Fig. 4). However, these nephelines had very different overall compositions (see Fig. 3), with NP-K-2 having a large K concentration in the nepheline. Furthermore, nepheline composition of NP-K-2 is relatively enriched in K compared to the starting melt composition (Fig. 4). This nepheline was still relatively enriched in Na compared to the starting melts (Fig. 4), but much less so than the other measured nephelines, suggesting that the K is substituting in nepheline preferentially despite the availability of similar amounts of Na as the other NP glasses. One possible explanation for the high Fe content may be that NP-K-2 and NP-Fe-3 featured the highest values for excess alkali (i.e., $\text{Na}+\text{K}-\text{Al}$ from Table 4) to charge compensate AlO_4

tetrahedral units, meaning that more alkali is available to charge balance the formation of FeO_4 tetrahedral units. This trend does not hold when Ca is taken into consideration, however, probably because Ca incorporation requires vacancy creation. However, assessment of the role of iron is problematic due to potential redox changes in Fe.

The amount of Fe that enters the nepheline structure will depend upon melt composition and how much iron-containing spinel forms upon cooling. Generally speaking, when HLW glass melts cool, spinels, usually mixed spinel but similar to magnetite or trevorite, with some additional Mn and Cr, will form first, followed by nepheline (Jantzen and Brown 2007b). Therefore, a portion of the Fe from the melt will be consumed before nepheline has the opportunity to crystallize. A small portion of Al can also be consumed by spinel, but it is insignificant compared to Fe unless the glasses are highly concentrated in Al_2O_3 , in which case an Al-based spinel has been observed to form (Smith et al. 2014). As such, it may be helpful to take advantage of this crystallization sequence, since, unlike nepheline, spinel does not negatively impact the durability of the remaining glass phase (Bailey and Hrma 1995).

Overall, Al and Na moderately increased in concentration in the crystal relative to the starting melt. Additionally, Fe and K and possibly Ca increased in the crystal as this component concentration increased in the starting melt composition. Silica is normally enriched in the residual glass relative to the crystal, since Si/Al is approximately unity for nepheline, and nuclear waste glass melts never have equimolar Al and Si due to excessively high melting temperatures and viscosities. Therefore, even if all Al goes into nepheline, there is still residual Si in the glass. It has been observed, however, that more nepheline can crystallize from the melt than starting Al concentration would predict (Menkhaus et al. 2000), again suggesting excess Si in nepheline, as is often seen in geological samples. In our case, A4 has much less Si than the NP samples, and still produces nepheline enriched in Si.

However, the behavior of Si itself in these samples is complex, as the SEM-EDS maps of Figure 5 show. In NP-K-2 there exists a silicon-rich phase in addition to nepheline, embedded between nepheline branches. From the micrographs in Figure 2 it is apparent that a similar phase also exists in A4 and NP-Li-2 at least, if not in all the samples. Further work is required to determine the nature of this phase, its role in crystallization, and its presence or absence in other glasses.

IMPLICATIONS

Five compositionally varied simulated high-level nuclear waste glasses, known to crystallize large fractions of nepheline on slow cooling, were investigated to assess the role of starting melt composition on resultant nepheline crystal composition. Nepheline is known to be compositionally flexible in its incorporation of many cations and vacancies, but this apparently does not extend to the substitution of B in the glasses studied here. Two crystallized glasses whose nephelines were found with significant Ca fractions featured starting melt compositions that were lowest in total alkali elements. Based on the need for charge compensation, introduction of Ca into nepheline also introduced vacancies. Yet, the largest influence on the estimated vacancy concentration

in nepheline was the concentration of silica. Depending on the glass composition, Fe and K were enriched or depleted in the residual glass, but always different from the starting melt.

More work is needed to observe the effects of starting melt composition on crystallization within simplified glasses of 3 to 5 components. Assessing the individual effects of Ca, Li, B, and Fe when combined with Na, Al, and Si in oxide melts of the nepheline stoichiometry will lend insight into the compositional partitioning between melt and nepheline crystal, and the resulting viscosity of the residual melt at the interface of the growing crystal and its effect on crystal growth. Also important will be understanding the role of phosphorus-containing and silica-rich (possibly lithium-containing) phases observed here. Increased recognition of the compositional aspects of crystallization in the nepheline system through the techniques featured in this work could also yield useful data for the formulation of commercial glass and glass ceramics beyond the nepheline system, such as those in the commercially important eucryptite-spodumene system. In addition, the EPMA technique used here to carefully quantify B with the use of LDE6 analyzing crystal is recommended for compositional analysis of natural specimens and commercial glasses with low boron. The modeling provided in this work aimed to calculate the effect of starting melt composition on the vacancy concentration in nepheline, and should provide further information on the corrosion susceptibility of the residual glass phase after crystallization. Ultimately, understanding of the chemical nature of nepheline crystallized from borosilicate melts is critical to be able to accurately model residual glass composition following slow cooling, and hence long-term durability of nuclear waste glass in geological repositories.

ACKNOWLEDGMENTS

This research was supported by the Department of Energy's Waste Treatment and Immobilization Plant Federal Project Office, contract number DE-EM0002904, under the direction of Albert A. Kruger. Further support for José Marcial was provided by the Graduate Assistance in Areas of National Need (GAANN) fellowship. Electron microprobe analyses were performed at the Peter Hooper GeoAnalytical Laboratory of the Washington State University School of the Environment. The authors thank the two anonymous reviewers and the editor for suggestions that substantially improved the manuscript.

REFERENCES CITED

- Akatov, A.A., Nikonov, B.S., Omel'yanenko, B.I., Stefanovskaya, O.I., Stefanovsky, S.V., Sunstov, D.Y., and Marra, J.C. (2010) Influence of the content of a surrogate of iron aluminate high-level wastes on the phase composition and structure of glassy materials for their immobilization. *Glass Physics and Chemistry*, 36, 45–52.
- Amoroso, J. (2011) Computer modeling of high-level waste glass temperatures within DWPF canisters during pouring and cool down. SRNL-STI-2011-00546, Savannah River National Laboratory, Aiken, South Carolina.
- Antao, S.M., and Hassan, I. (2010) Nepheline: Structure of three samples from the Bancroft area, Ontario, obtained using synchrotron high-resolution powder X-ray diffraction. *Canadian Mineralogist*, 48, 69–80.
- ASTM (2008) Standard Test Methods for Determining Chemical Durability of Nuclear, Hazardous, and Mixed Waste Glasses and Multiphase Glass Ceramics: The Product Consistency Test (PCT). ASTM Committee C26 on Nuclear Fuel Cycle. ASTM International, West Conshohocken, Pennsylvania.
- Bailey, A.W., and Hrma, P. (1995) Waste loading maximization for vitrified Hanford HLW blend. *Ceramic Transactions*, 61, Environmental Issues and Waste Management Technologies, 549–556. American Ceramic Society, Westerville, OH.
- Bastin, G.F., and Heijligers, H.J.M. (1991) Quantitative electron probe microanalysis of nitrogen. *Scanning*, 13, 325–342.
- Blancher, S.B., D'Arco, P., Fontelles, M., and Pascal, M.-L. (2010) Evolution of nepheline from mafic to highly differentiated members of the alkaline series: the Messum complex, Namibia. *Mineralogical Magazine*, 74, 415–432.
- Bourcier, W.L. (1998) Affinity Functions for Modeling Glass Dissolution Rates. UCRL-JC-131186, Lawrence Livermore National Laboratory, Livermore, CA.
- Buerger, M.J., Klein, G.E., and Donnay, G. (1954) Determination of the crystal structure of nepheline. *American Mineralogist*, 39, 805–818.
- Deer, W.A., Howie, R.A., Wise, W.S., and Zussman, J. (2004) *Framework Silicates: Silica Minerals, Feldspatoids and the Zeolites*. The Geological Society, London.
- Dollase, W.A., and Thomas, W.M. (1978) The crystal chemistry of silica-rich, alkali-deficient nepheline. *Contributions to Mineralogy and Petrology*, 66, 311–318.
- Donnay, G., Schairer, J.F., and Donnay, J.D.H. (1959) Nepheline solid solutions. *Mineralogical Magazine*, 32, 93–109.
- Donovan, J.J. (2014) *Probe for EPMA v. 10.4.5, User's Guide and Reference*, Xtreme Edition.
- Duffy, J.A., and Ingram, M.D. (1976) An interpretation of glass chemistry in terms of the optical basicity concept. *Journal of Non-Crystalline Solids*, 21, 373–410.
- Fox, K.M., Edwards, T.B., and Peeler, D.K. (2008) Control of nepheline crystallization in nuclear waste glass. *International Journal of Applied Ceramic Technology*, 5, 666–673.
- Friese, K., Grzechnik, A., Petříček, V., Schönleber, A., van Smaalen, S., and Morgenroth, W. (2011) Modulated structure of nepheline. *Acta Crystallographica*, B67, 18–29.
- Goldschmidt, V.M. (1937) The principles of distribution of chemical elements in minerals and rocks. The seventh Hugo Muller Lecture, delivered before the Chemical Society on March 17th, 1937. *Journal of the Chemical Society (Resumed)*, 655–673.
- Hamilton, J.P., Pantano, C.G., and Brantley, S.L. (2000) Dissolution of albite glass and crystal. *Geochimica et Cosmochimica Acta*, 64, 2603–2615.
- Horny, P., Lifshin, E., Campbell, H., and Gauvin, R. (2010) Development of a New Quantitative X-Ray Microanalysis Method for Electron Microscopy. *Microscopy and Microanalysis*, 16, 821–830.
- Hrma, P. (2010) Crystallization during processing of nuclear waste glass. *Journal of Non-Crystalline Solids*, 356, 3019–3025.
- Hrma, P., Schweiger, M.J., Humrickhouse, C.J., Moody, J.A., Tate, R.M., Rainsdon, T.T., TeGrotenhuis, N.E., Arrigoni, B.M., Marcial, J., Rodriguez, C.P., and Tincher, B.H. (2010) Effect of glass-batch makeup on the melting process. *Ceramics-Silikaty*, 54, 193–211.
- Hrma, P., Riley, B.J., Crum, J.V., and Matyas, J. (2014) The effect of high-level waste glass composition on spinel liquidus temperature. *Journal of Non-Crystalline Solids*, 384, 32–40.
- Jantzen, C.M., and Brown, K.G. (2007a) Predicting the spinel-nepheline liquidus for application to nuclear waste glass processing. Part I: Primary phase analysis, liquidus measurement, and quasicrystalline approach. *Journal of the American Ceramic Society*, 90, 1866–1879.
- (2007b) Predicting the spinel-nepheline liquidus for application to nuclear waste glass processing. Part II: Quasicrystalline freezing point depression model. *Journal of the American Ceramic Society*, 90, 1880–1891.
- Jantzen, C.M., Brown, K.G., and Pickett, J.B. (2010) Durable glass for thousands of years. *International Journal of Applied Glass Science*, 1, 38–62.
- Kim, D.S., Schweiger, M.J., Rodriguez, C.P., Lepry, W.C., Lang, J.B., Crum, J.D., Vienna, J.D., Johnson, F.C., Marra, J.C., and Peeler, D.K. (2011) Formulation and Characterization of Waste Glasses with Varying Processing Temperature. PNNL-20774, EMSP-RPT-009, Pacific Northwest National Laboratory, Richland, WA.
- Kirkpatrick, R.J. (1975) Crystal Growth from melt: a review. *American Mineralogist*, 60, 798–814.
- Kobayashi, H., Toda, K., Kohno, H., Arai, T., and Wilson, R. (1995) The study of some peculiar phenomena in ultra-soft X-ray measurements using synthetic multilayer crystals. *Advances in X-ray Analysis*, 307–312.
- Krause, J., Harlov, D.E., Pushkarev, E.V., and Brüggmann, G.E. (2013) Apatite and clinopyroxene as tracers for metasomatic processes in nepheline clinopyroxenites of Uralian-Alaskan-type complexes in the Ural Mountains, Russian Federation. *Geochimica et Cosmochimica Acta*, 121, 503–521.
- Lambotte, G., and Chartrand, P. (2013) Thermodynamic modeling of the (Al₂O₃+Na₂O), (Al₂O₃+Na₂O+SiO₂), and (Al₂O₃+Na₂O+AlF₃+NaF) systems. *The Journal of Chemical Thermodynamics*, 57, 306–334.
- Li, H., Vienna, J.D., Hrma, P., Smith, D.E., and Schweiger, M.J. (1997) Nepheline precipitation in high-level waste glasses: compositional effects and impact on the waste form acceptability. In W.J. Gray and I.R. Triay, Eds., *Proceedings of MRS, 465, Scientific Basis for Nuclear Waste Management XX*, p. 261–268. Materials Research Society, Pittsburgh, Pennsylvania.
- Li, H., Hrma, P., Vienna, J.D., Qian, M., Su, Y., and Smith, D.E. (2003) Effects of Al₂O₃, B₂O₃, Na₂O, and SiO₂ on nepheline formation in borosilicate glasses: chemical and physical correlations. *Journal of Non-Crystalline Solids*, 331, 202–216.
- Malinina, G.A., Stefanovsky, S.V., and Stefanovskaya, O.I. (2012) Phase composition and structure of boron-free and boron-containing sodium aluminum iron silicate glass materials for solid radioactive waste immobilization. *Glass Physics and Chemistry*, 38, 280–289.
- Matsumoto, M., Tomeoka, K., Seto, Y., Miyake, A., and Sugita, M. (2014) Nepheline and sodalite in the matrix of the Ningqiang carbonaceous chondrite:

- Implications for formation through parent-body processes. *Geochimica et Cosmochimica Acta*, 126, 441–454.
- Matyáš, J., Vienna, J.D., Kimura, A., Schaible, M., and Tate, R.M. (2010) Development of Crystal-Tolerant Waste Glasses. *Advances in Materials Science for Environmental and Nuclear Technology*, p. 41–50. Wiley, New York.
- McCloy, J., and Vienna, J.D. (2010a) Glass Composition Constraint Recommendations for Use in Life-Cycle Mission Modeling. PNNL-19372, Pacific Northwest National Laboratory, Richland, Washington.
- (2010b) Glass Composition Constraint Recommendations for use in Life-Cycle Mission Modeling. PNNL-19372, Pacific Northwest National Laboratory, Richland, WA.
- McCloy, J.S., Schweiger, M.J., Rodriguez, C.P., and Vienna, J.D. (2011) Nepheline crystallization in nuclear waste glasses: Progress toward acceptance of high-alumina formulations. *International Journal of Applied Glass Science*, 2, 201–214.
- McCloy, J., Washton, N., Gassman, P., Marcial, J., Weaver, J., and Kukkadapu, R. (2015) Nepheline crystallization in boron-rich aluminosilicate glasses as investigated by multi-nuclear NMR, Raman, and Mössbauer spectroscopies. *Journal of Non-Crystalline Solids*, 409, 149–165.
- McGee, J.J., and Anovitz, L.M. (1996) Electron probe microanalysis of geologic materials for boron. In L.M. Anovitz, and E.S. Grew, Eds., *Boron: Mineralogy, Petrology, and Geochemistry*, vol. 33, p. 771–788. Reviews in Mineralogy, Petrology and Geochemistry, Mineralogical Society of America, Chantilly, Virginia.
- McGee, J.J., Slack, J.F., and Herrington, C.R. (1991) Boron analysis by electron microprobe using MoB₃C layered synthetic crystals. *American Mineralogist*, 76, 681–684.
- McKeown, D.A. (2005) Raman spectroscopy and vibrational analyses of albite: From 25 °C through the melting temperature. *American Mineralogist*, 90, 1506–1517.
- Menkhaus, T.J., Hrma, P., and Li, H. (2000) Kinetics of nepheline crystallization from high-level waste glass. In G.T. Chandler and X. Feng, Eds., *Ceramic Transactions, 107, Environmental Issues and Waste Management Technologies in the Ceramic and Nuclear Industries V*, p. 461–468. American Ceramic Society, Westerville, Ohio.
- Newbury, D.E. (2005) Misidentification of major constituents by automatic qualitative energy dispersive X-ray microanalysis: A problem that threatens the credibility of the analytical community. *Microscopy and Microanalysis*, 11, 545–561.
- Newbury, D.E., and Ritchie, N.W.M. (2013) Is scanning electron microscopy/energy dispersive X-ray spectrometry (SEM/EDS) quantitative? *Scanning*, 35, 141–168.
- Newbury, D.E., Swyt, C.R., and Myklebust, R.L. (1995) “Standardless” Quantitative Electron Probe Microanalysis with Energy-Dispersive X-ray Spectrometry: Is It Worth the Risk? *Analytical Chemistry*, 67, 1866–1871.
- Onuma, K., Iwai, T., and Kenzo, Y. (1972) Nepheline—“iron nepheline” solid solutions. *Journal of the Faculty of Science, Hokkaido University, Series 4, Geology and Mineralogy*, 15, 179–190.
- Ota, T., Yamai, I., and Hayashi, T. (1995) Nepheline gradient solid solutions. *Journal of Materials Science*, 30, 2701–2705.
- Pierce, E.M., Reed, L.R., Shaw, W.J., McGrail, B.P., Icenhower, J.P., Windisch, C.F., Cordova, E.A., and Broady, J. (2010) Experimental determination of the effect of the ratio of B/Al on glass dissolution along the nepheline (NaAlSi₃O₈)-malkoite (NaBSi₃O₈) join. *Geochimica et Cosmochimica Acta*, 74, 2634–2654.
- Raudsepp, M. (1995) Recent advances in the electron-probe micro-analysis of minerals for the light elements. *Canadian Mineralogist*, 33, 203–218.
- Riley, B.J., Hrma, P., Rosario, J., and Vienna, J.D. (2001a) Effect of Crystallization on High-Level Waste Glass Corrosion. In G.L. Smith, S.K. Sundaram, and D.R. Spearing, Eds., *Ceramic Transactions, Environmental Issues and Waste Management Technologies in the Ceramic and Nuclear Industries VII*, 132, p. 257–265. The American Ceramic Society.
- Riley, B.J., Rosaria, J.A., and Hrma, P. (2001b) Impact of HLW Glass Crystallinity on PCT Response. PNNL-13491, Pacific Northwest National Laboratory, Richland, Washington.
- Rodriguez, C.P., McCloy, J., Schweiger, M.J., Crum, J.V., and Winschell, A. (2011) Optical basicity and nepheline crystallization in high alumina glasses. PNNL-20184, Pacific Northwest National Laboratory, Richland, Washington.
- Rossi, G., Oberti, R., and Smith, D.C. (1989) The crystal structure of a K-poor Ca-rich silicate with the nepheline framework, and crystal-chemical relationships in the compositional space (K,Na,Ca)₈(Al, Si)₁₆O₃₂. *European Journal of Mineralogy*, 1, 59–70.
- Smith, G., Kim, D.-S., Schweiger, M., Lang, J., Crum, J., Crawford, C., Vienna, J., and Marra, J. (2014) Silicate Based Glass Formulations for Immobilization of U.S. Defense Wastes Using Cold Crucible Induction Melters. PNNL-23288, Pacific Northwest National Laboratory, Richland, Washington.
- Stebbins, J.F., Murdoch, J.B., Carmichael, I.S.E., and Pines, A. (1986) Defects and short-range order in nepheline group minerals: a silicon-29 nuclear magnetic resonance study. *Physics and Chemistry of Minerals*, 13, 371–381.
- Steele, I.M., and Pluth, J.J. (1990) Crystal structure of synthetic yoshiokaite, a stuffed derivative of the tridymite structure. *American Mineralogist*, 75, 1186–1191.
- Stefanovsky, S.V., and Marra, J.C. (2007) The effect of waste loading on the structure and leach resistance of borosilicate glass for Savannah River Site SB2 waste immobilization. WM’07 Waste Management Conference, Tucson, Arizona.
- (2011) The Effect of Waste Loading and Glass Structural Factors on Structure and Chemical Durability of SB2 and SB4 SRS Waste Glasses—11397. WM2011 Conference, Phoenix, Arizona.
- Stefanovsky, S.V., Lebedev, V.V., Sunstov, D.Y., Nikonov, B.S., Omel’yanenko, B.I., Akatov, A.A., and Marra, J.C. (2010) Influence of the content of radioactive wastes with high concentrations of aluminum, sodium, and iron oxides on the phase composition and structure of glassy materials prepared in a “cold crucible”. *Glass Physics and Chemistry*, 36, 419–430.
- Sugiyama, K., Shinkai, T., and Waseda, Y. (1998) Structural Study of Molten Albite (NaAlSi₃O₈) by the High Temperature Energy Dispersive X-ray Diffraction (EDXD) Method. *High Temperature Materials and Processes*, 17, 155–162.
- Tait, K.T., Sokolova, E., and Hawthorne, F.C. (2003) The Crystal Chemistry of Nepheline. *Canadian Mineralogist*, 41, 61–70.
- Taylor, M., and Brown, G.E. Jr. (1979) Structure of mineral glasses—I. The feldspar glasses NaAlSi₃O₈, KAlSi₃O₈, CaAl₂Si₂O₈. *Geochimica et Cosmochimica Acta*, 43, 61–75.
- Taylor, M., Brown, G.E. Jr., and Fenn, P.M. (1980) Structure of mineral glasses—III. NaAlSi₃O₈ supercooled liquid at 805°C and the effects of thermal history. *Geochimica et Cosmochimica Acta*, 44, 109–117.
- Upadhyay, D. (2012) Alteration of plagioclase to nepheline in the Khariar alkaline complex, SE India: Constraints on metasomatic replacement reaction mechanisms. *Lithos*, 155, 19–29.
- Vienna, J.D., Skorski, D.C., Kim, D.S., and Matyáš, J. (2013) Glass Property Models and Constraints for Estimating the Glass to be Produced at Hanford by Implementing Current Advanced Glass Formulation Efforts. U.S. Department of Energy Report EWG-RPT-003, Pacific Northwest National Laboratory, Richland, Washington.
- Vulić, P., Balić-Zunić, T., Belmonte, L., and Kahlenberg, V. (2011) Crystal chemistry of nephelines from ijolites and nepheline-rich pegmatites: influence of composition and genesis on the crystal structure investigated by X-ray diffraction. *Mineralogy and Petrology*, 101, 185–194.

MANUSCRIPT RECEIVED APRIL 2, 2015

MANUSCRIPT ACCEPTED AUGUST 12, 2015

MANUSCRIPT HANDLED BY DANIEL NEUVILLE